NACA TN 2674

TECH LIBRARY KAFB, NM
0065460

# NATIONAL ADVISORY COMMITTEE FOR AERONAUTICS

TECHNICAL NOTE 2674

## SOME EXPERIMENTS ON VISUALIZATION OF FLOW FIELDS BEHIND LOW-ASPECT-RATIO WINGS BY MEANS OF A TUFT GRID

By John D. Bird and Donald R. Riley

Langley Aeronautical Laboratory
Langley Field, Va.

Washington
May 1952

319.98/9

AFMDC
TECHNICAL LIBRARY
AFL 2811

PERMANENT

TECH LIBRARY KAFB, NM

0065460

NATIONAL ADVISORY COMMITTEE FOR AERONAUTICS

TECHNICAL NOTE 2674

# SOME EXPERIMENTS ON VISUALIZATION OF FLOW FIELDS BEHIND LOW-ASPECT-RATIO WINGS BY MEANS OF A TUFT GRID

By John D. Bird and Donald R. Riley

## SUMMARY

A technique for obtaining a physical picture of the flow behind a wing, combination of wings, or other aircraft components is described. This technique involves photographing from far downstream the action of a large number of tufts of uniform length mounted on a screen. This procedure permits obtaining, in an approximate fashion, an important result of a pitot-yaw-head survey; namely, a vector plot of the flow field in a plane normal to the air stream at a station downstream of an aerodynamic surface. A preliminary examination of the tuft-grid technique as discussed in this paper indicates that quantitative analyses concerning such factors as trailing-vortex strength and location, approximate downwash and sidewash angles over a large field behind lifting surfaces and other aerodynamic forms may be satisfactorily conducted with the data obtained by this technique.

## INTRODUCTION

Present trends in aerodynamic design are toward the use of unorthodox wing plan forms, lower aspect ratios, and unusual combinations of lifting surfaces. These trends are particularly evident in missile design where low-aspect-ratio cruciform arrangements and tandem surfaces of approximately equal area are commonly encountered. A good understanding of the complicated flow fields existing in the vicinity and downstream of these lifting-surface arrangements is necessary in order to provide for an optimum choice of geometry and, in particular, for an optimum placement of rear surfaces relative to those in front.

A technique for obtaining a physical picture of the flow field behind a wing, combination of wings, or other airplane components has been developed in the Langley stability tunnel. This technique involves photographing from far downstream the action of a large number of tufts of uniform length mounted on a screen. This procedure permits, in an

approximate fashion, obtaining an important result of a pitot-yaw-head survey; namely, a vector plot of the flow field in a plane normal to the air stream at a station behind an aerodynamic surface. In this sense, a tuft grid should be particularly useful in the instruction of aerodynamics and in furnishing at least approximate downwash and sidewash data over a large area behind wings. Tufts have, of course, frequently been employed as an aid to visualizing flow in the vicinity of aerodynamic shapes and in various forms of wind channels. References 1 and 2 describe the use of tufts in recording the downwash and general flow character behind lifting surfaces by making photographs of tufts suspended on wires. These photographs were made along a line about normal to the free stream and are an excellent means for establishing approximate downwash angles with a minimum of labor.

A preliminary study of the application of the tuft-grid technique for visualization of the flow field behind several low-aspect-ratio wings has been completed and some of the results of this study are presented herein. Surface-tuft photographs and some force data, obtained at the same dynamic pressure, are also presented to provide a broader interpretation of the results. No attempt has been made to analyze the results in a quantitative manner, although such analyses are practical.

## SYMBOLS

The force and moment data presented herein are in the form of standard NACA coefficients which are referred to the system of axes shown in figure 1. The origin of the axis system coincides with the plane of symmetry and the quarter chord of the mean aerodynamic chord. The coefficients and symbols are defined as follows:

$C_L$ lift coefficient $\left(\frac{\text{Lift}}{qS}\right)$

$C_D$ drag coefficient $\left(\frac{\text{Drag}}{qS}\right)$

$C_m$ pitching-moment coefficient $\left(\frac{M}{qS\bar{c}}\right)$

$M$ pitching moment about wing mounting point

$q$ dynamic pressure

$S$ wing area

| | |
|---|---|
| $\bar{c}$ | wing mean aerodynamic chord |
| $\alpha_T$ | uncorrected angle of attack |
| $\alpha$ | angle of attack |
| $\beta$ | angle of sideslip |
| $x'$ | distance from trailing edge to wing mounting point |

## APPARATUS, MODELS, AND TESTS

### Description of Tuft Grid

The tuft grid employed in this investigation consisted essentially of a rectangular grid of fine wires (0.012-in. diameter) of 1-inch mesh supported at the periphery by a tubular framework with 3-inch woolen tufts attached at the intersections of the wires. The tufted area of the grid was 50 inches wide and 26 inches high. A preloading system consisting of a spring mounted between one end of each wire and the frame was used to maintain a 1.5-pound tension in each wire. Each intersection of a vertical and a horizontal wire was soldered so that relative movement between wires would be eliminated.

The tufts were of 4-ply-wool baby yarn and were attached to the grid with strong thread. A small loop of thread was provided at the attaching point in order to permit the tuft to move freely in all directions. The downstream end of each tuft was tied with thread to prevent the strands of wool from unraveling. A close-range photograph showing the wires and tufts of the tuft grid is presented as figure 2.

A truss-like structure was welded to each of the rectangular frame members to provide a fairly rigid frame. The frame and truss-like structure were fashioned from thin-wall streamline tubing having a 0.75-inch chord. Mounting brackets were located at each of the four corners for attaching the frame to the supporting system used in the tunnel.

The supporting system included two vertical members constructed from streamline tubing to which the mounting brackets were attached. The attachments were such that the tuft grid could be located at any desired vertical position. Four pieces of 2-inch angle iron, each 3 feet in length and placed parallel to the air stream - two were bolted to the tunnel ceiling and two, to the tunnel floor - provided a means for locating the grid at any desired station downstream of the model. A photograph of the tuft grid and its supporting system located behind

a 75° triangular wing at 20° angle of attack is presented in figure 3. The four shields located in the corners contain the lights which provide illumination for photography. As the tufts indicate, the tunnel was in operation when this photograph was taken.

## Testing Procedure

A cutaway view of a section of a wind tunnel showing the general location of the camera, the tuft grid, and the model is presented in figure 4(a). The camera can only record the projections of the tufts and model in a vertical plane. Still or motion-picture cameras may be used for photographing the grid. The still camera used for these tests was an automatic aerial camera with a 20-inch-focal-length lens. A standard motion-picture camera was used for a portion of the tests. The cameras were placed 60 feet downstream of the tuft grid for all tests in order to minimize parallax. An illustrative example of the type of picture obtained by a still camera is shown in figure 4(b). In this figure the gray triangular area represents the vertical projection of a triangular-wing model operating at an angle of attack. The short dark lines represent the tufts. In the relatively undisturbed regions of flow, the tufts appear as short dark lines or dots (see the center of the top horizontal row) and in the disturbed regions, as longer lines. One of the tufts in the sketch has been magnified for the purpose of illustration. The vertical and horizontal projections of each tuft together with the tuft length (3 in. for this grid) determine the downwash and sidewash angles of the flow at a given location.

A practical limit of accuracy of the tuft grid employed in this investigation is believed to be $\pm\frac{1}{2}^{\circ}$ of angle for an individual tuft for regions of reasonably steady flow. Parallax causes an error of about 2° at the edge of the grid and must be accounted for in actual measurements of downwash and sidewash. At a specific point, however, actual determination of the change in downwash caused by some small model modification, such as filleting, could better be accomplished by the use of a pitot-yaw head.

## Models

A total of six wings were tested in this investigation. The pertinent geometric and aerodynamic properties of these wings are listed in table I. For all the test configurations, the wings had a strip of white masking tape on the trailing edge which photographed as a solid white line.

## Tests

All the tests, including the force and moment tests, were conducted in the 6- by 6-foot test section of the Langley stability tunnel at a dynamic pressure of 8 pounds per square foot, which corresponds to a velocity of approximately 58 miles per hour and to Reynolds numbers from 630,000 to 1,400,000 based on the mean aerodynamic chord. Data were obtained for the rectangular wing, the 45°, 60°, and 75° triangular wings, each having an NACA 0012 airfoil section, through the angle-of-attack range for zero yaw. For the 60° triangular wing having an NACA $65_{(06)}$-006.5 airfoil section, data were obtained through the angle-of-attack range for various angles of yaw and through the yaw range for various angles of attack. An angle-of-attack run for this same wing was obtained with 10-percent all-moving half-delta tip controls deflected -20°. Figure 5 presents some of the lift, drag, and pitching-moment characteristics as a function of angle of attack at zero sideslip for the rectangular and the 45°, 60°, and 75° triangular wings. Representative tuft-grid and surface-tuft photographs are presented for all tests made.

Yawing oscillation tests were conducted for a 60° triangular wing which was made of $\frac{3}{4}$-inch plywood with rounding near the leading edge and an 8° bevel at the trailing edge. Tuft-grid photographs were obtained by using a 16-millimeter movie camera for an oscillation frequency of about 1 cycle per second for the tuft grid located 6 inches downstream of the wing trailing edge. A series of enlarged photographs taken from movie film are presented for this frequency.

The force and moment data have been corrected for the effect of the jet boundaries by the following formulas:

$$\Delta\alpha = 57.3\ \delta\ \frac{S}{C}\ C_L$$

$$\Delta C_D = \delta\ \frac{S}{C}\ C_L{}^2$$

where

| | |
|---|---|
| $\Delta\alpha$ | correction to angle of attack |
| $\Delta C_D$ | correction to drag coefficient |
| S | wing area, square feet |
| C | wind-tunnel cross-sectional area (36 sq ft) |

The jet-boundary correction factor $\delta$ for the wings listed in table I is as follows:

| Wings: | $\delta$ |
|---|---|
| Rectangular | 0.145 |
| $45^{\circ}$ triangular | 0.154 |
| $60^{\circ}$ triangular | 0.145 |
| $75^{\circ}$ triangular | 0.140 |

No corrections, however, have been applied for blocking, turbulence, or support-strut interference, and no attempt has been made to correct for distortion of the flow fields by the tunnel walls.

## RESULTS AND DISCUSSION

### Angle-of-Attack Variations at Zero Yaw

Rectangular wing.- The tuft-grid and surface-tuft photographs for the rectangular wing are presented in figures 6 and 7, respectively. The solid white line in figure 6 represents the wing trailing edge and moves downward with respect to the grid as the angle of attack is increased. The trailing vortices begin to form near the wing tips as evidenced at both grid locations for $\alpha_T = 8^{\circ}$. A line of shear indicating the presence of the trailing-vortex sheet may be seen near the trailing edge at this angle of attack for the 6-inch grid location. This shear does not show at the 24-inch station or at higher angles of attack, presumably because the degree of roll-up of the vortex sheet is proportional to the distance behind the wing and the lift coefficient. The increase in vortex strength at higher angles of attack is indicated by the growth of the area influenced by the vortices. Throughout the angle-of-attack range, the trailing vortices remain near the wing tips for this particular plan form. For a given angle of attack, little variation is apparent between the photographs for the two grid locations except at $\alpha_T = 18^{\circ}$. Lift and pitching-moment data (fig. 5) indicate that a stall occurred slightly above $\alpha = 16^{\circ}$. The surface-tuft photograph for $\alpha_T = 18^{\circ}$ indicates that the stall occurred near the wing center section. The stall is also apparent on the tuft-grid pictures for $\alpha_T = 18^{\circ}$ as evidenced by an erratic behavior of the tufts near the center of the wing span.

The behavior of the tufts at $\alpha_T = 18^{\circ}$ was of the nature that would be obtained from a three-dimensional form of the von Kármán vortex street, wherein the discharged vorticity appears as a trail of ring vortices. This effect has been more graphically illustrated by motion pictures of the pattern on a tuft grid mounted behind a long 2-inch by 4-inch timber.

In this case, a fluctuating spanwise pattern, indicating both a spanwise as well as a streamwise distribution of ring vortices, is shown. The existence of this behavior would be expected to be dependent on the Reynolds number in much the same manner as for the two-dimensional case.

The significant differences in the tuft-grid pictures of two tail lengths at $\alpha_T = 18^\circ$ are the amount of area on the tuft grid influenced by the stall and the behavior of the tufts. The tufts at the 6-inch station appear to be moving much more violently than at the 24-inch station, as would be expected.

$45^\circ$ triangular wing.- Tuft-grid and surface-tuft pictures for the triangular wing having the leading edges swept back $45^\circ$ are presented in figures 8 and 9. The trailing vortices are first seen near the wing tips at $8^\circ$ angle of attack as indicated in figure 8 for both grid locations rearward of the model. For the 24-inch station, both vortices are slightly above the tips. At $\alpha_T = 12^\circ$, the surface tufts show that a small region on either tip has developed a rough flow that is directed generally outward; this behavior indicates an inward movement of the trailing vortices. At $\alpha_T = 16^\circ$ and $20^\circ$, the area of the wing covered by the rough flow has increased. The tuft grid for both the 6- and 24-inch stations clearly indicate the unsteady flow field and inward movement of the trailing-vortex system for $\alpha_T = 16^\circ$ and $20^\circ$. For these test conditions, this particular leading-edge sweep appears to be a critical one where the tip stall is accompanied by a sudden inward movement of the trailing-vortex system. The nature of the trailing-vortex system of this and the other wings tested is in general agreement with the results indicated by higher-scale wind-tunnel investigations. (See reference 3.)

$60^\circ$ triangular wing.- The tuft-grid and surface-tuft photographs for the $60^\circ$ triangular wing, having an NACA 0012 airfoil section, are presented in figures 10 and 11. The inward movement of the vortices from the tips is very evident as the angle of attack is increased. (See fig. 10.) For $\alpha_T = 32^\circ$, the wing is approaching the angle of attack for maximum lift, hence, the rather violent pattern indicated for the 6-inch station. Some difference exists between the 6- and 24-inch stations for $\alpha_T = 16^\circ$. For the 24-inch station, the pattern on the grid below the wing trailing edge indicates a triangular area of almost pure downwash, the lower limit of which is believed to define the trailing-vortex sheet. This sheet is slightly above the intersection of the wing chord plane with the tuft grid. For the 6-inch station, the vortex sheet is much less deflected, as may be noted from the line of shear near the trailing edge, and this region of pure downwash is almost nonexistent. The surface tufts for $\alpha_T = 24^\circ$ and $32^\circ$ indicate the

unsteadiness associated with the inward movement of the trailing-vortex system near the leading edge of the tip sections. This unsteadiness can also be detected at the outer edges of the wing in the tuft-grid photographs.

75° triangular wing.- The tuft-grid and surface-tuft photographs for the 75° triangular wing are presented in figures 12 and 13. The surface-tuft photographs (fig. 13) for $\alpha_T = 16^\circ$, $20^\circ$, and $32^\circ$ indicate narrow well-defined bands on both the left and right semispans of the wing where the tufts are pointing toward the tips. This region locates the trailing vortices as they leave the apex and sweep back across the wing inside of the leading edges and slightly above the wing surface. No evidence of an unsteady flow is apparent for this wing in either the surface-tuft or tuft-grid photographs. The lift data (fig. 5) indicate that the angle of attack for maximum lift is above the range of angles tested in this investigation. For this degree of leading-edge sweep, the trailing vortices, as indicated by the tuft grid, remain essentially in the same location as the angle of attack is increased. The triangular area of almost pure downwash (no sidewash) is also apparent for this wing (see $\alpha_T = 16^\circ$).

## Effect of Sideslip

Figure 14 presents tuft-grid photographs through the angle-of-attack range for a 60° triangular wing having an NACA $65_{(06)}$-006.5 airfoil section for values of the angle of sideslip of 0°, -5°, -10°, and -20° and a grid location of 24 inches downstream of the model. For the condition of zero sideslip, the trailing vortices move inboard from the tips as the angle of attack is increased, as was noted for the 60° triangular wing with NACA 0012 section. For sideslip angles of -5°, -10°, and -20°, the vortex leaving the tip of the leading semispan moves inboard from the tip as the angle of attack is increased. The vortex leaving the trailing semispan, however, remained in about the same location relative to the wing tip for all angles of attack at a given angle of sideslip. Shown in figure 15 are surface-tuft photographs, showing the effect of sideslipping the wing model while at a constant angle of attack. Evidence of an above-surface vortex flow is increased on the retreating semispan, and evidence of tip stalling is increased on the advancing semispan as the angle of sideslip is increased.

## Deflecting Tip Controls

Tuft-grid and surface-tuft photographs for the 60° triangular wing having an NACA $65_{(06)}$-006.5 airfoil section with 10-percent half-delta

all-moving tip controls deflected -20° are presented in figures 16 and 17. Figure 16 shows two vortices originating at either edge of each control at zero angle of attack. At the 24-inch station, for both 0° and 4° angles of attack, the vortices appear to be slightly farther above the control surface than for the 6-inch station. As the angle of attack of the wing is increased, however, the two primary vortices of the wing become apparent and the tip-control vortices disappear.

### Yawing Oscillation Tests

In order to determine the general applicability of the tuft grid in providing physical interpretations of various forms of flow fields, photographs were obtained for a 60° flat-plate-section triangular wing oscillating in yaw through ±12° at a frequency of about 1 cycle per second. The wing model was at an angle of attack of 21°, and the tuft grid was located 6 inches downstream of the wing trailing edge. The data were recorded by means of a 16-millimeter movie camera operating at about 75 frames per second. Various frames during the oscillation were enlarged and are presented in figure 18. The time lag between the occurrence of a particular flow pattern at the wing trailing edge and at the tuft grid is about 0.01 second so that this factor is of little importance for this sequence of pictures.

An interesting character is apparent in the behavior of the trailing-vortex system for this oscillating wing. The rough flow field that develops in the vicinity of the out-going tip near maximum amplitude, as may be seen from figure 18, frames 21 to 25, persists until the model has returned and passed considerably beyond zero amplitude. (See wing tips in fig. 18, frames 1 to 5, 11 to 15, and 21 to 25.) This aerodynamic-lag effect is associated with semistalled flow and may be considerably different from that for purely potential flow.

## CONCLUDING REMARKS

A qualitative examination of the data obtained from the application of a tuft-grid flow visualization technique to the fields existing behind several low-aspect-ratio wings of rectangular and triangular plan forms indicated that the character of the flow field is in general agreement with what has been anticipated on the basis of higher-scale tests utilizing other techniques. The results indicated also that quantitative analyses concerning such factors as trailing-vortex strength and location, and approximate downwash and sidewash angles over a large area behind lifting surfaces and other aerodynamic forms may be satisfactorily conducted with data obtained by this technique. The use of

this tuft-grid technique should provide an excellent illustration of aerodynamic phenomena involving interaction between combinations of lifting surfaces and aerodynamic shapes.

Langley Aeronautical Laboratory
National Advisory Committee for Aeronautics
Langley Field, Va., January 11, 1952

## REFERENCES

1. Purser, Paul E., Spearman, M. Leroy, and Bates, William R.: Preliminary Investigation at Low Speed of Downwash Characteristics of Small-Scale Sweptback Wings. NACA TN 1378, 1947.

2. Schlichting, H.: Aerodynamics of the Mutual Influence of Aircraft Parts (Interference). Library Translation No. 275, British R.A.E., Oct. 1948.

3. Wick, Bradford H.: Chordwise and Spanwise Loadings Measured at Low Speed on a Triangular Wing Having an Aspect Ratio of Two and an NACA 0012 Airfoil Section. NACA TN 1650, 1948.

TABLE I.- GEOMETRIC CHARACTERISTICS OF WINGS INVESTIGATED

| Plan form | Sweep of leading edge (deg) | Aspect ratio | Wing span (in.) | $\bar{c}$ (in.) | S (sq in.) | Airfoil section parallel to chord plane of symmetry | Root chord (in.) | x' (in.) |
|---|---|---|---|---|---|---|---|---|
| | 45 | 4.0 | 48.0 | 16.0 | 576 | NACA 0012 | 24.0 | 12.0 |
| | 60 | 2.3 | 36.5 | 21.1 | 576 | NACA 0012 | 31.6 | 15.8 |
| | 75 | 1.1 | 24.8 | 30.9 | 576 | NACA 0012 | 46.4 | 23.2 |
| | 0 | 2.6 | 37.0 | 14.1 | 518 | NACA 0012 | 14.1 | 10.5 |
| 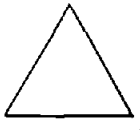 (a) | 60 | 2.3 | 36.5 | 21.1 | 576 | NACA $65_{(06)}$-006.5 | 31.6 | 15.8 |
| (b) | 60 | 2.3 | 36.5 | 21.1 | 576 | Flat plate | 31.6 | 15.8 |

[a]With and without 10-percent half-delta all-moving tip controls deflected.
[b]Used only in oscillation test.

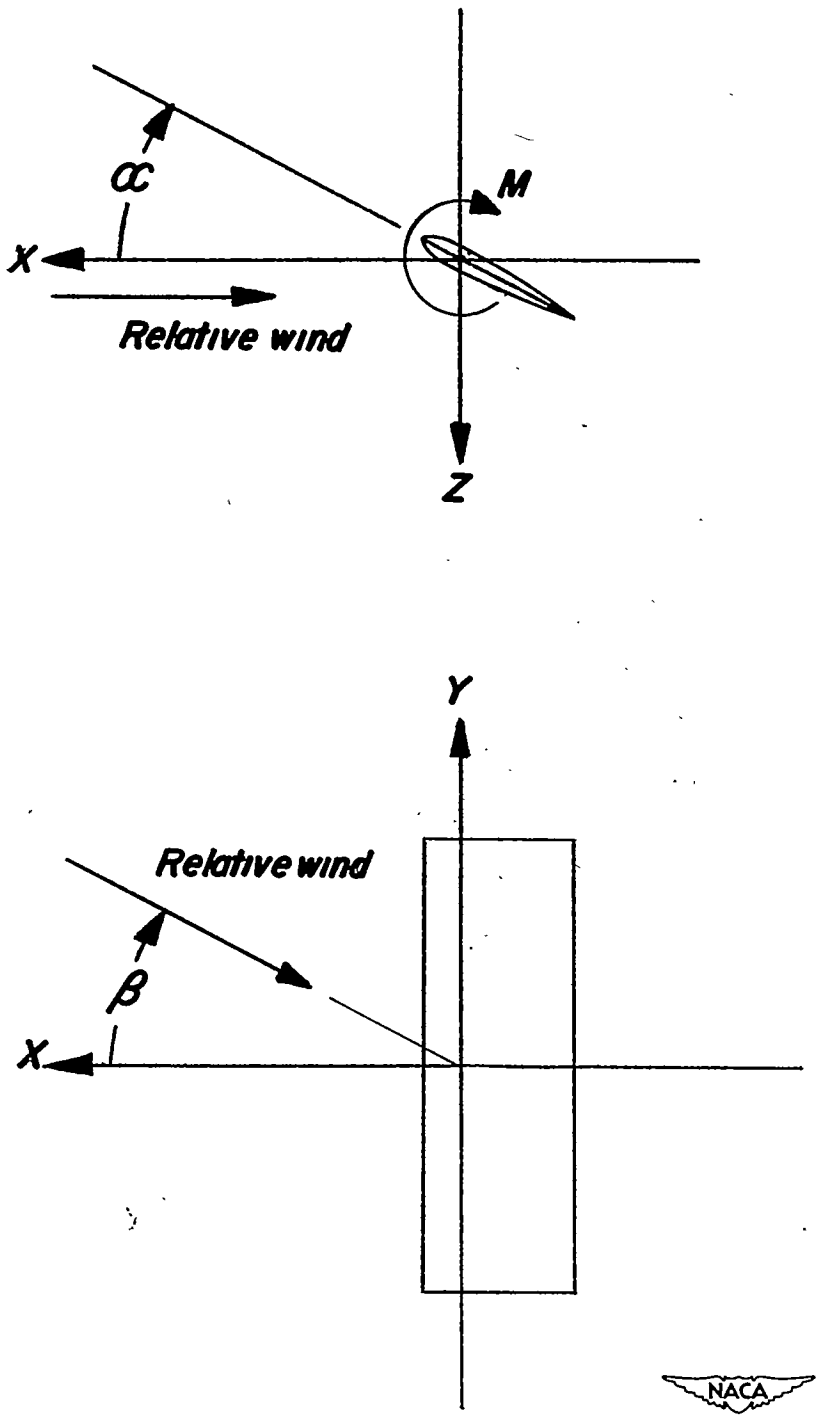


Figure 1.- System of axes employed in this paper.

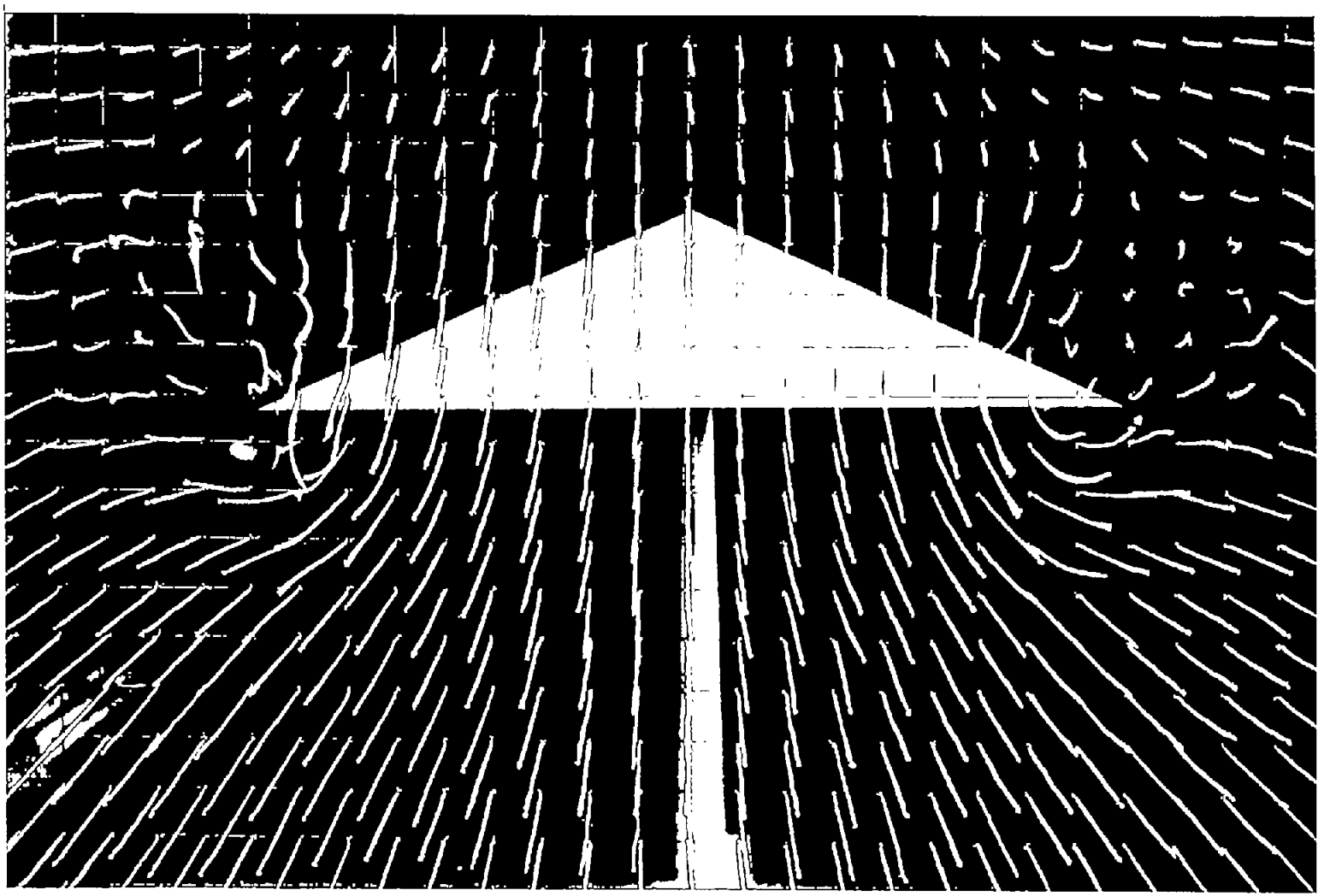

Figure 2.- Tuft grid viewed from close range.

NACA
L-70554

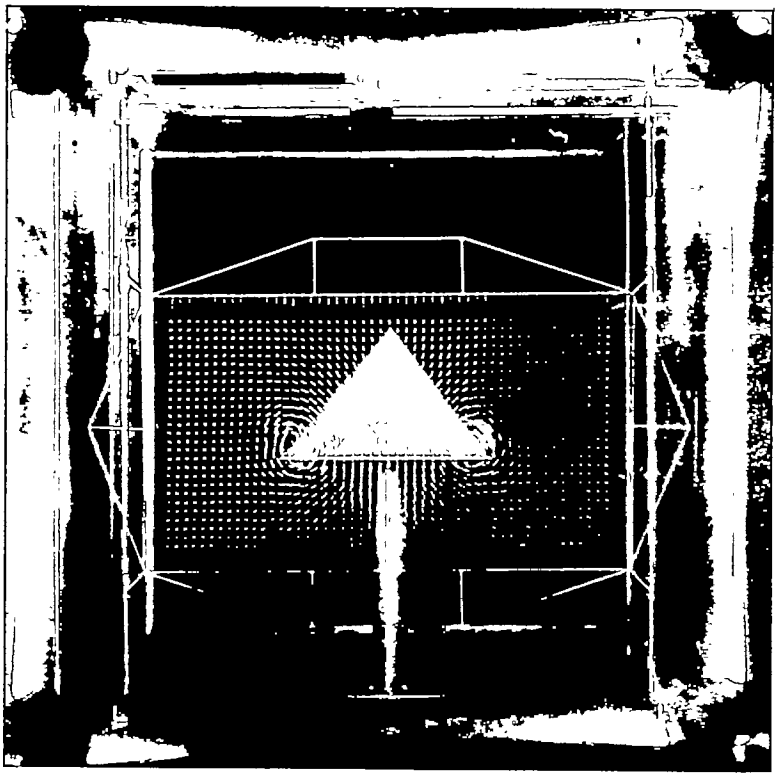

L-72718

Figure 3.- Tuft grid and supporting system located behind a 75° triangular wing at 20° angle of attack.

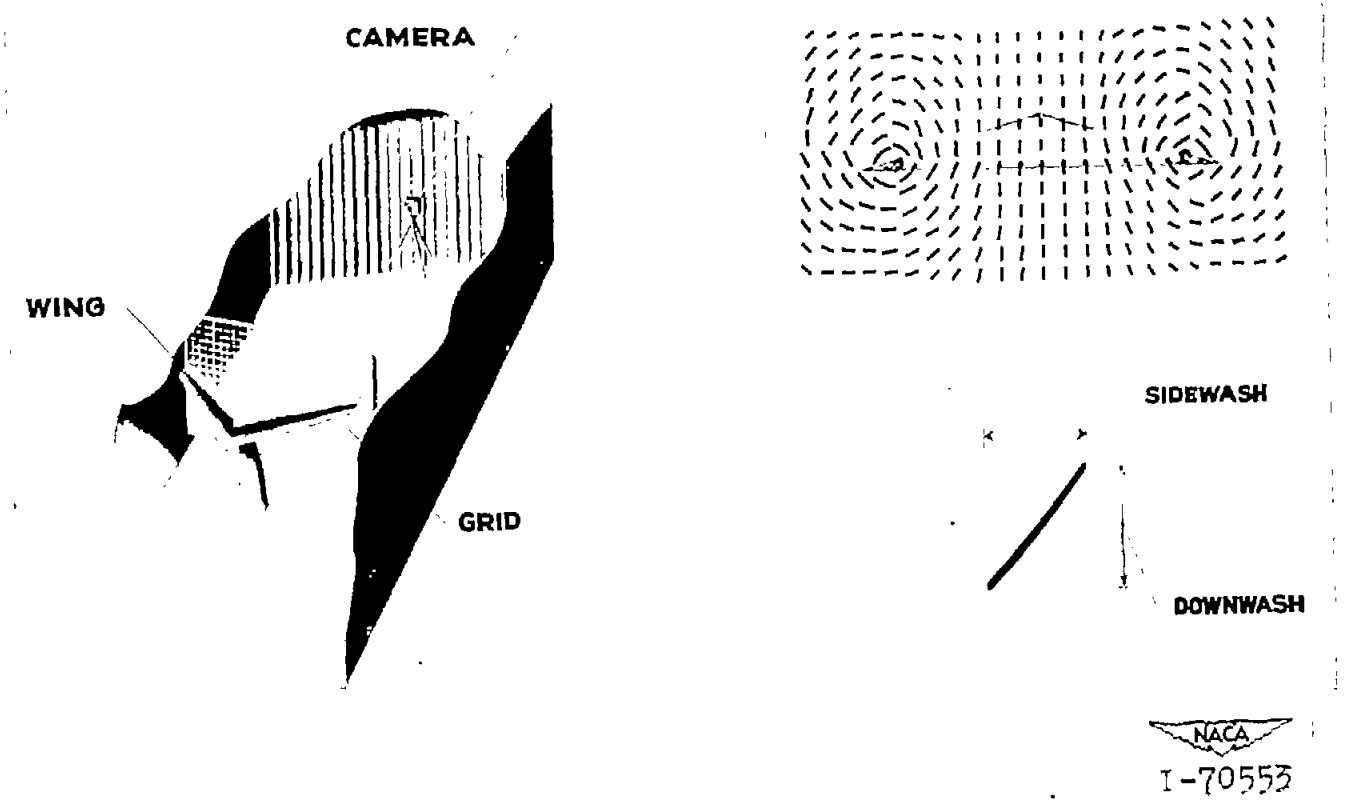


(a) Setup for flow surveys with tuft grid.

(b) Typical flow pattern for triangular wing.

Figure 4.- General arrangement of tuft-grid setup and interpretation of results as sidewash and downwash.

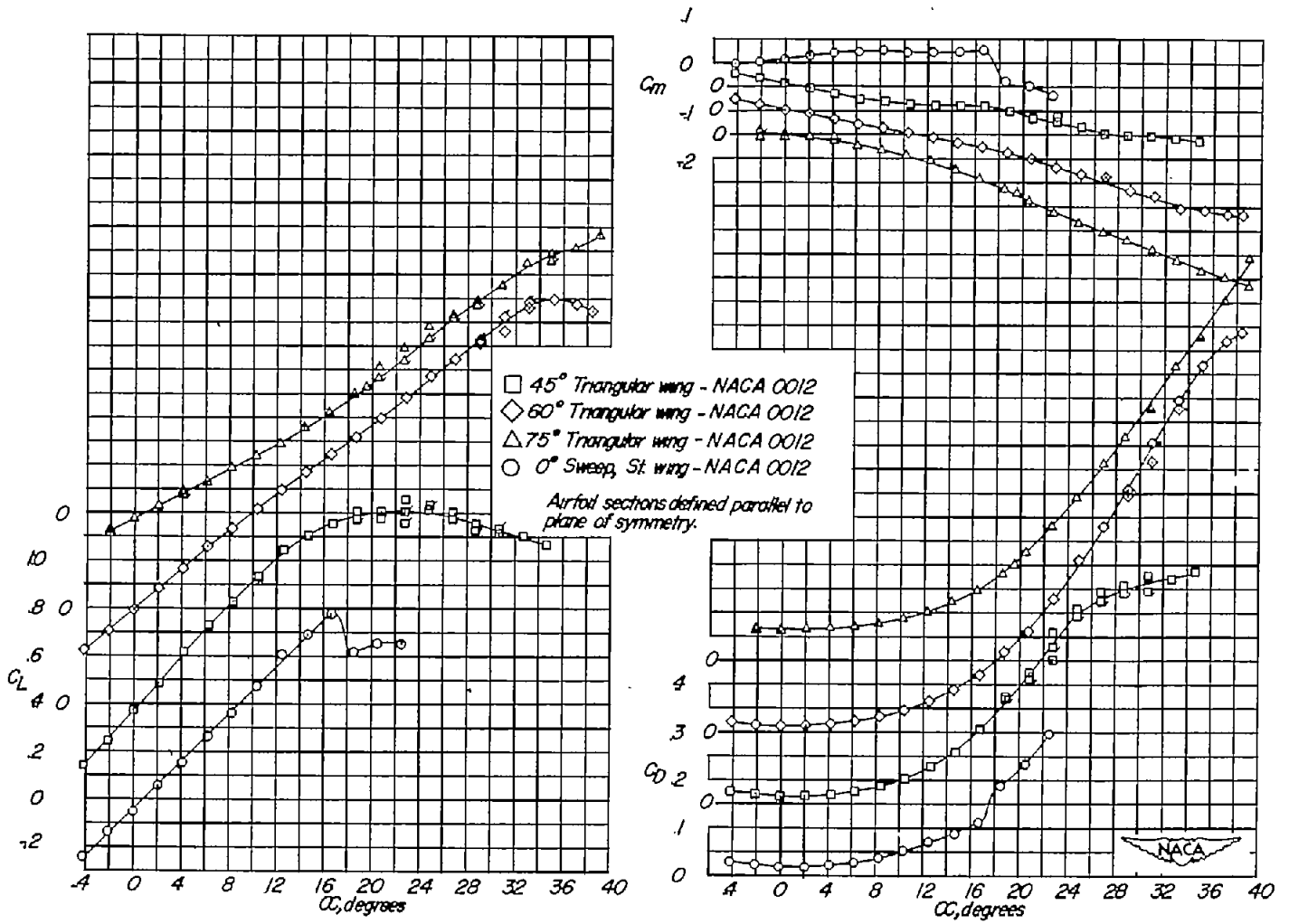


Figure 5.- The lift, drag, and pitching-moment characteristics as a function of angle of attack for the rectangular wing and the 45°, 60°, and 75° triangular wings. $\beta = 0°$.

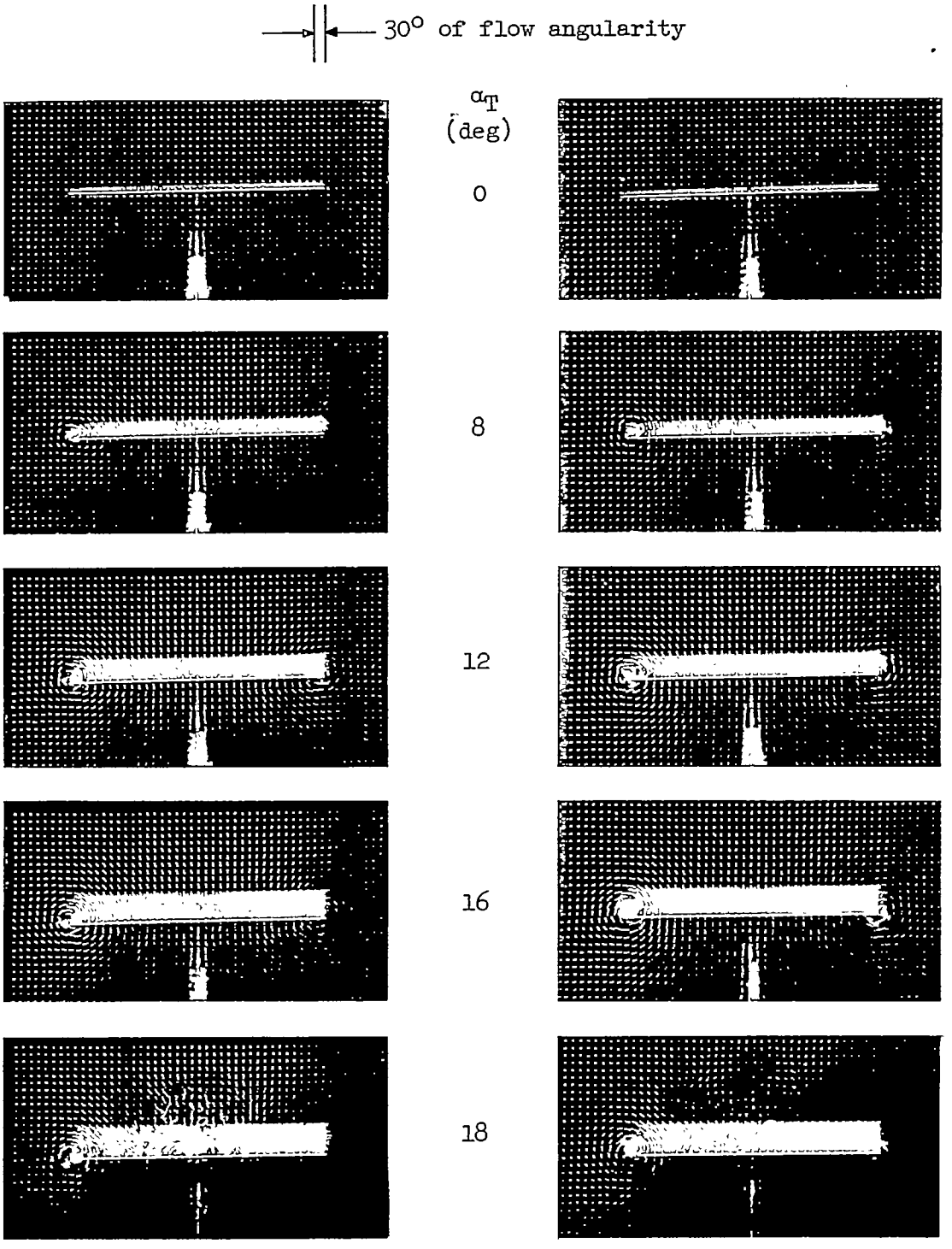


(a) Tuft grid 6 inches from trailing edge.

(b) Tuft grid 24 inches from trailing edge.

Figure 6.- Tuft-grid photographs for a rectangular wing of 2.31 aspect ratio with NACA 0012 airfoil section for two stations behind the wing. $\beta = 0^{\circ}$.

L-72719

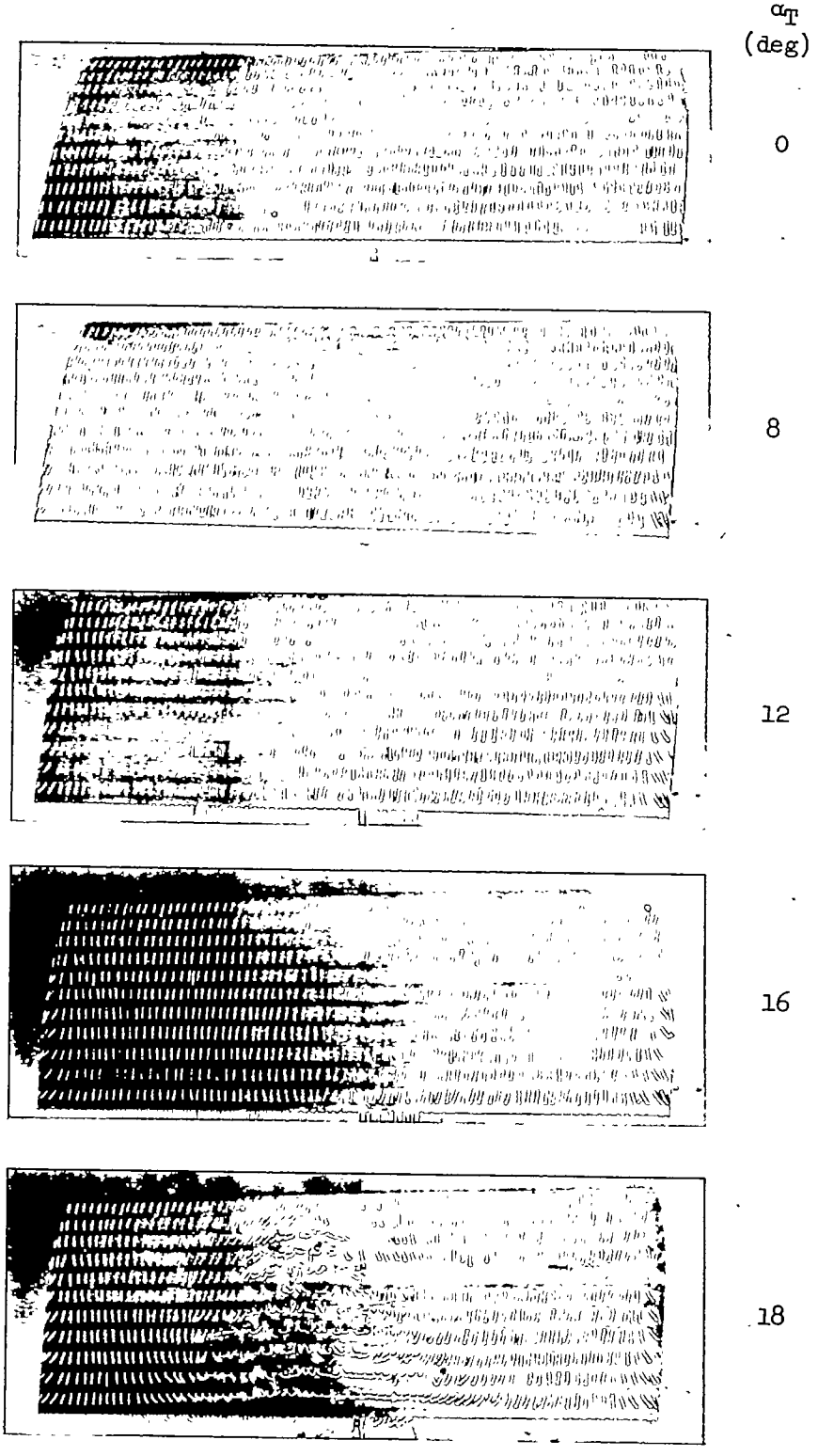


L-72720

Figure 7.- Surface-tuft photographs for a rectangular wing of 2.31 aspect ratio and NACA 0012 airfoil section. $\beta = 0^{\circ}$.

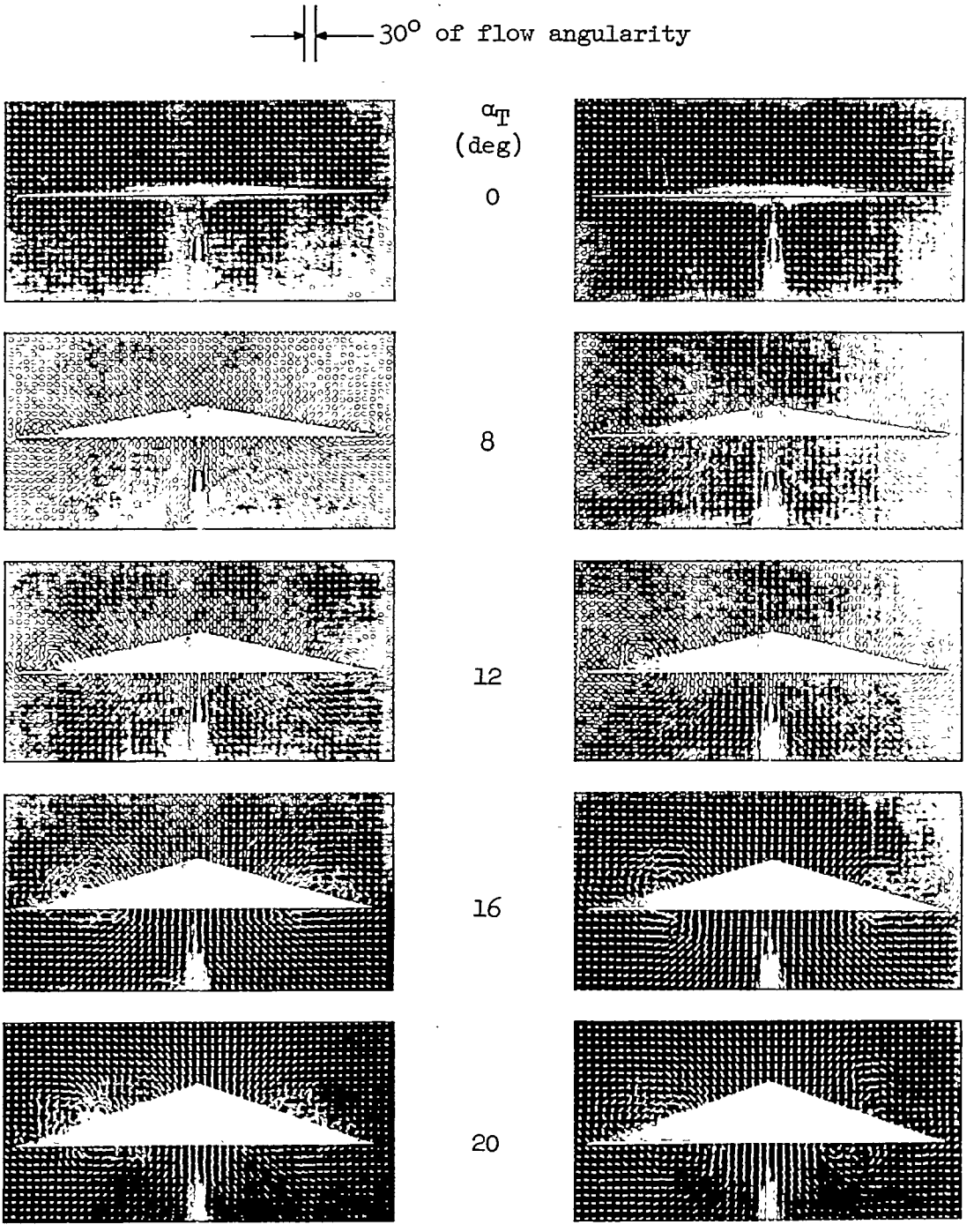


(a) Tuft grid 6 inches from trailing edge.

(b) Tuft grid 24 inches from trailing edge.

Figure 8.- Tuft-grid photographs for a 45° triangular wing with NACA 0012 airfoil section for two stations behind wing. $\beta = 0°$.

L-72721

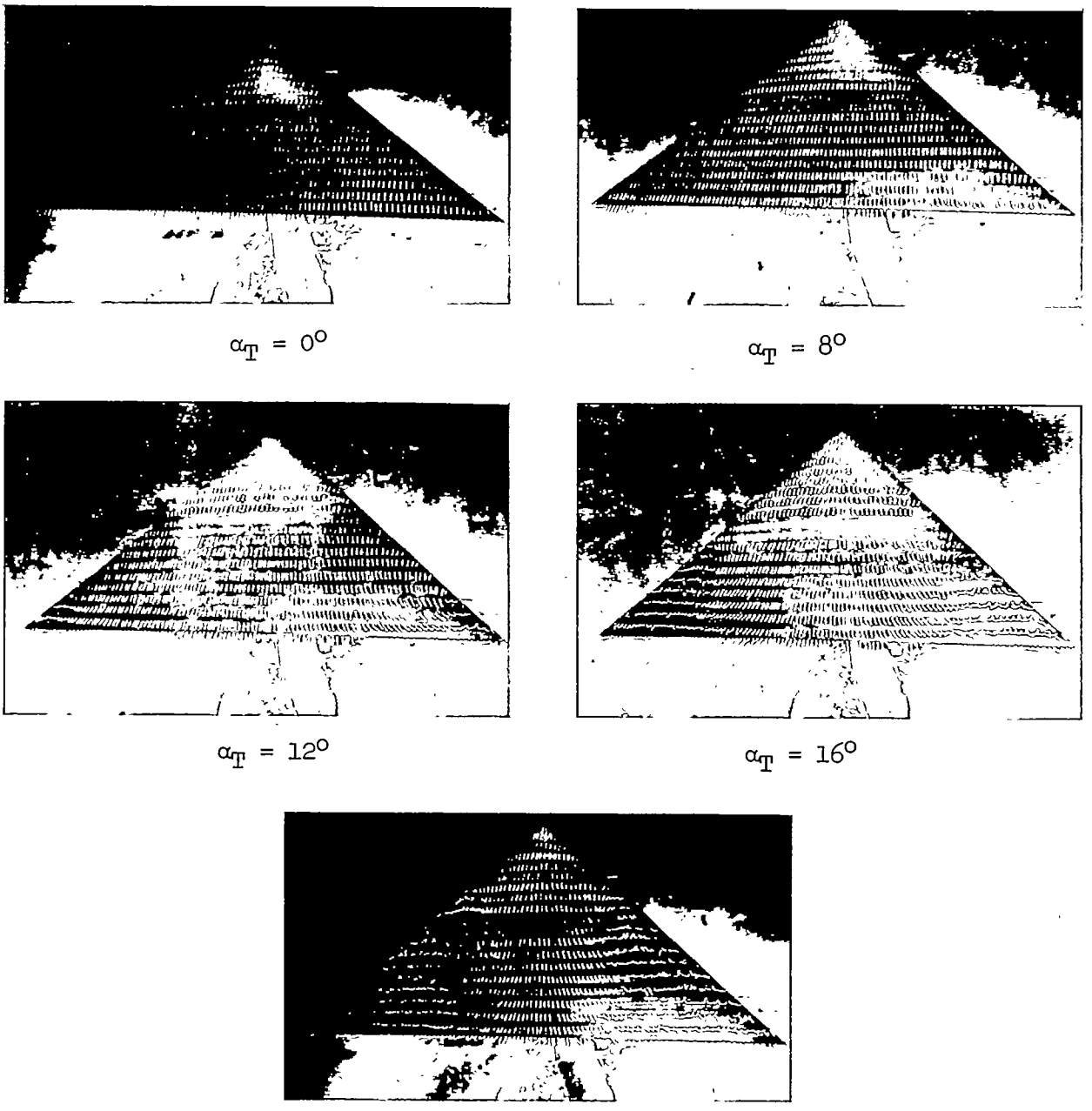


NACA
L-72722

Figure 9.- Surface-tuft photographs for a 45° triangular wing with NACA 0012 airfoil section. $\beta = 0^\circ$.

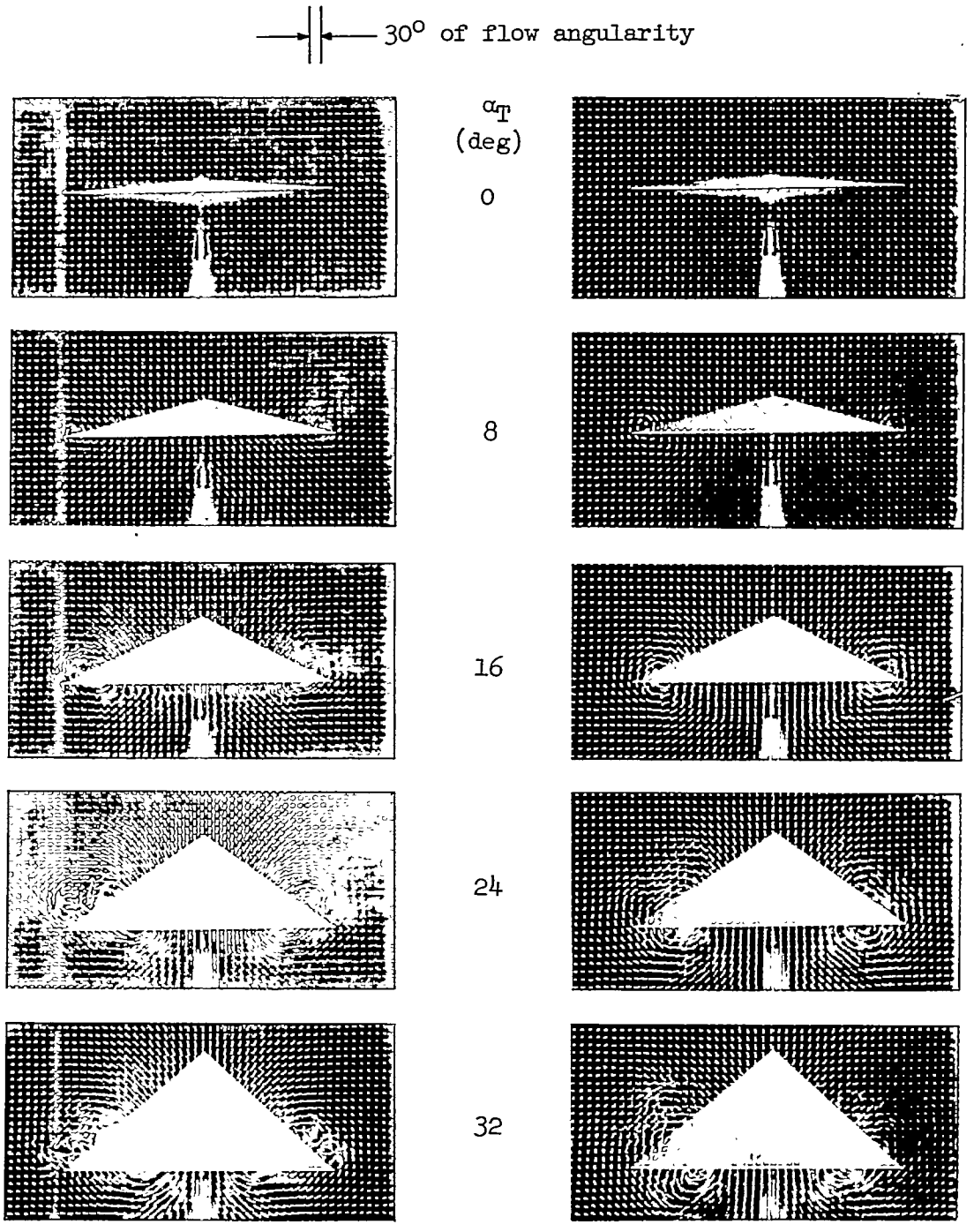


(a) Tuft grid 6 inches from trailing edge.

(b) Tuft grid 24 inches from trailing edge.

Figure 10.- Tuft-grid photographs for a 60° triangular wing with NACA 0012 airfoil section for two stations behind wing. $\beta = 0^{\circ}$.

L-72723

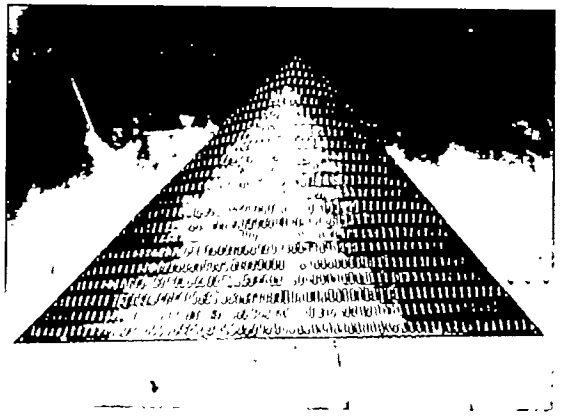

$\alpha_T = 0^\circ$

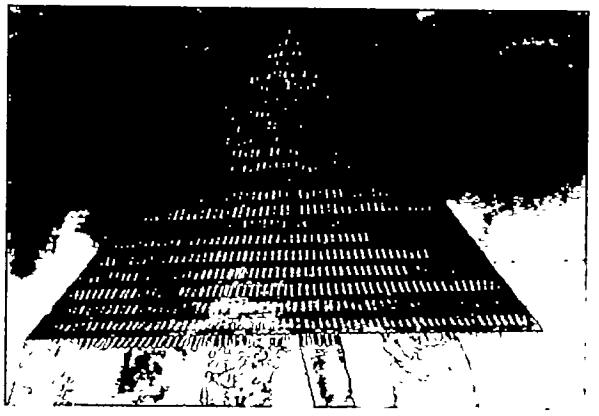

$\alpha_T = 8^\circ$

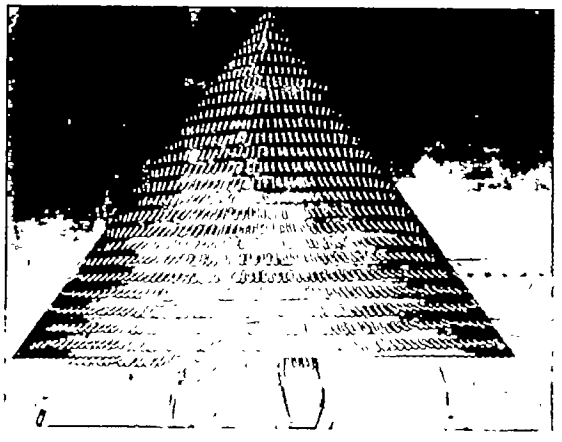

$\alpha_T = 16^\circ$

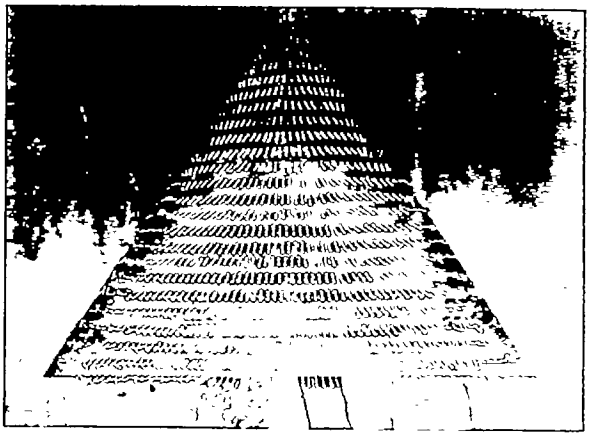

$\alpha_T = 24^\circ$

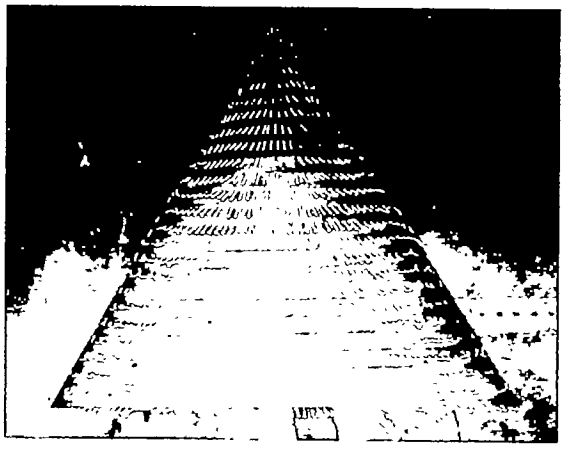

$\alpha_T = 32^\circ$

NACA
L-72724

Figure 11.- Surface-tuft photographs for a 60° triangular wing with NACA 0012 airfoil section. $\beta = 0^\circ$.

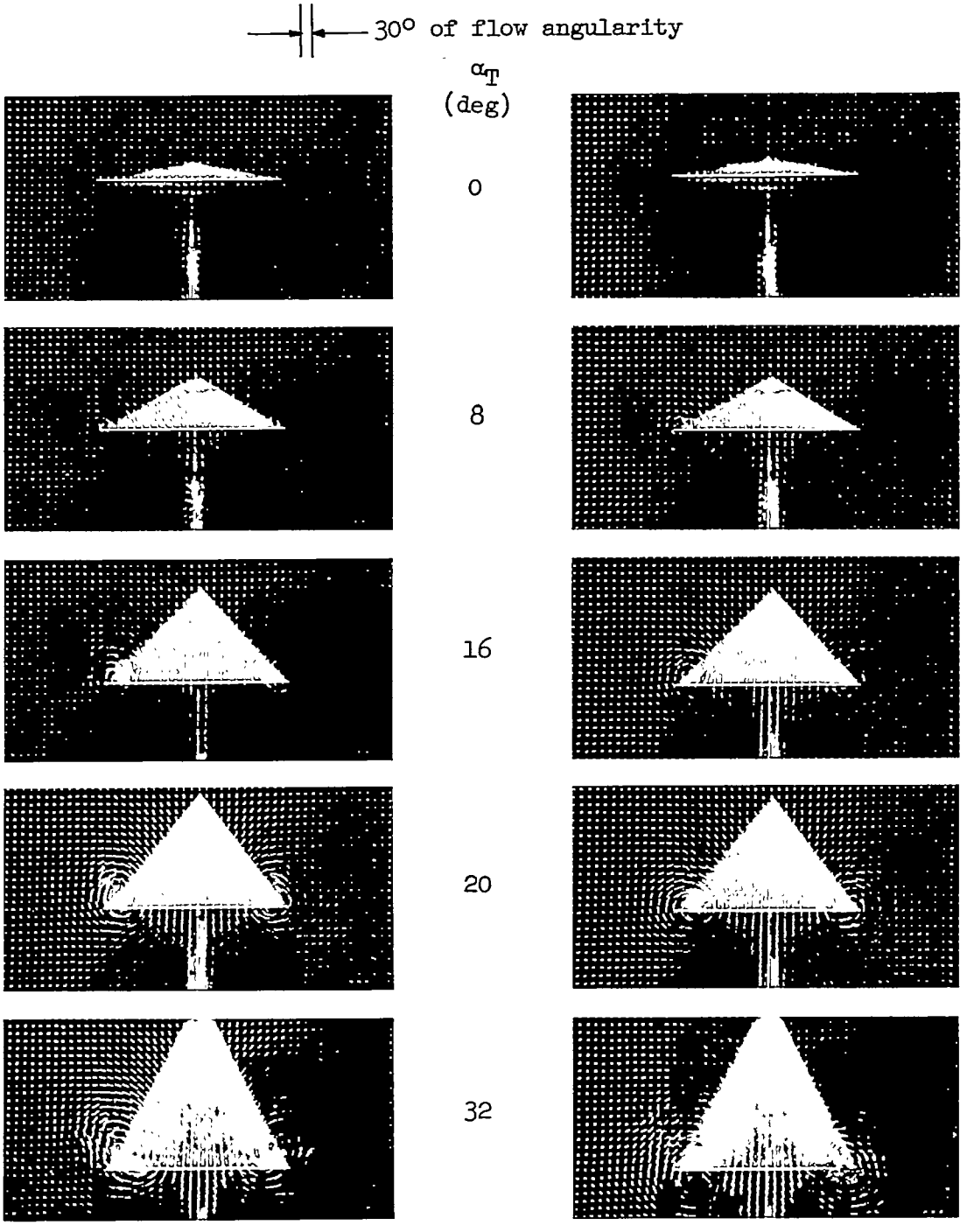


(a) Tuft grid 6 inches from trailing edge.

(b) Tuft grid 24 inches from trailing edge.

Figure 12.- Tuft-grid photographs for a 75° triangular wing with NACA 0012 airfoil section for two stations behind wing. $\beta = 0°$.

L-72725

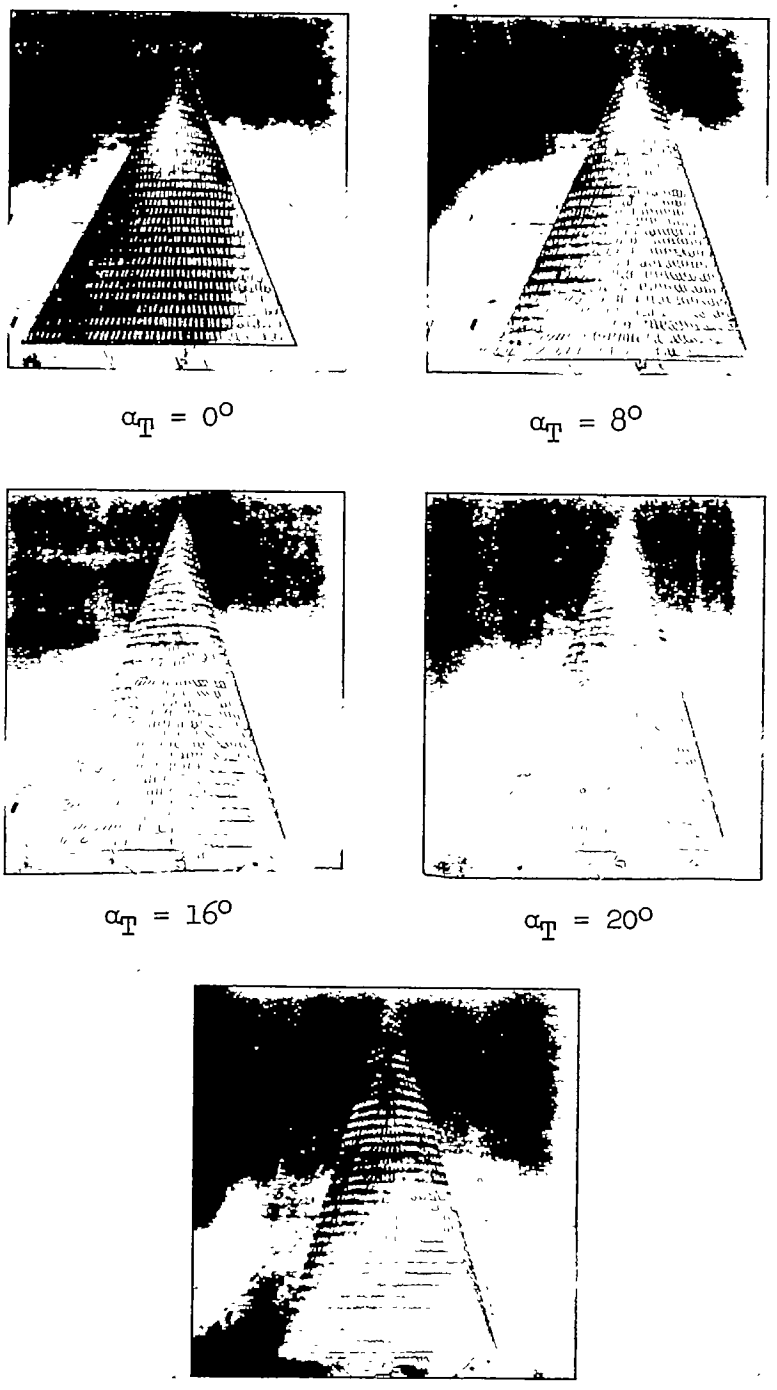


Figure 13.- Surface-tuft photographs for a 75° triangular wing with NACA 0012 airfoil section. $\beta = 0^\circ$.

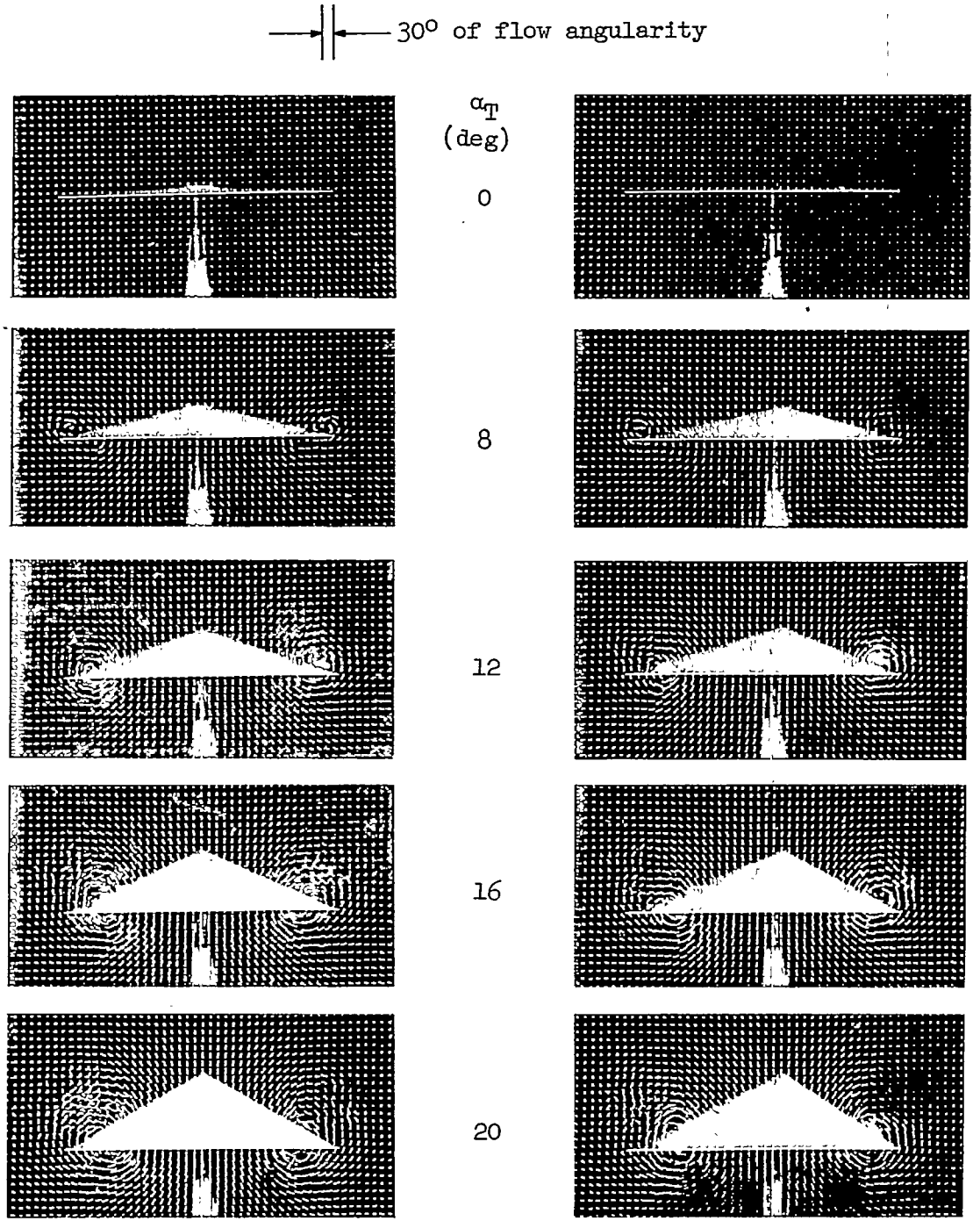


(a) $\beta = 0^{\circ}$.

(b) $\beta = -5^{\circ}$.

Figure 14.- Tuft-grid photographs for a 60° triangular wing having an NACA $65_{(06)}$-006.5 airfoil section at various combinations of angles of attack and sideslip. Tuft grid located 24 inches from wing trailing edge.

L-72727

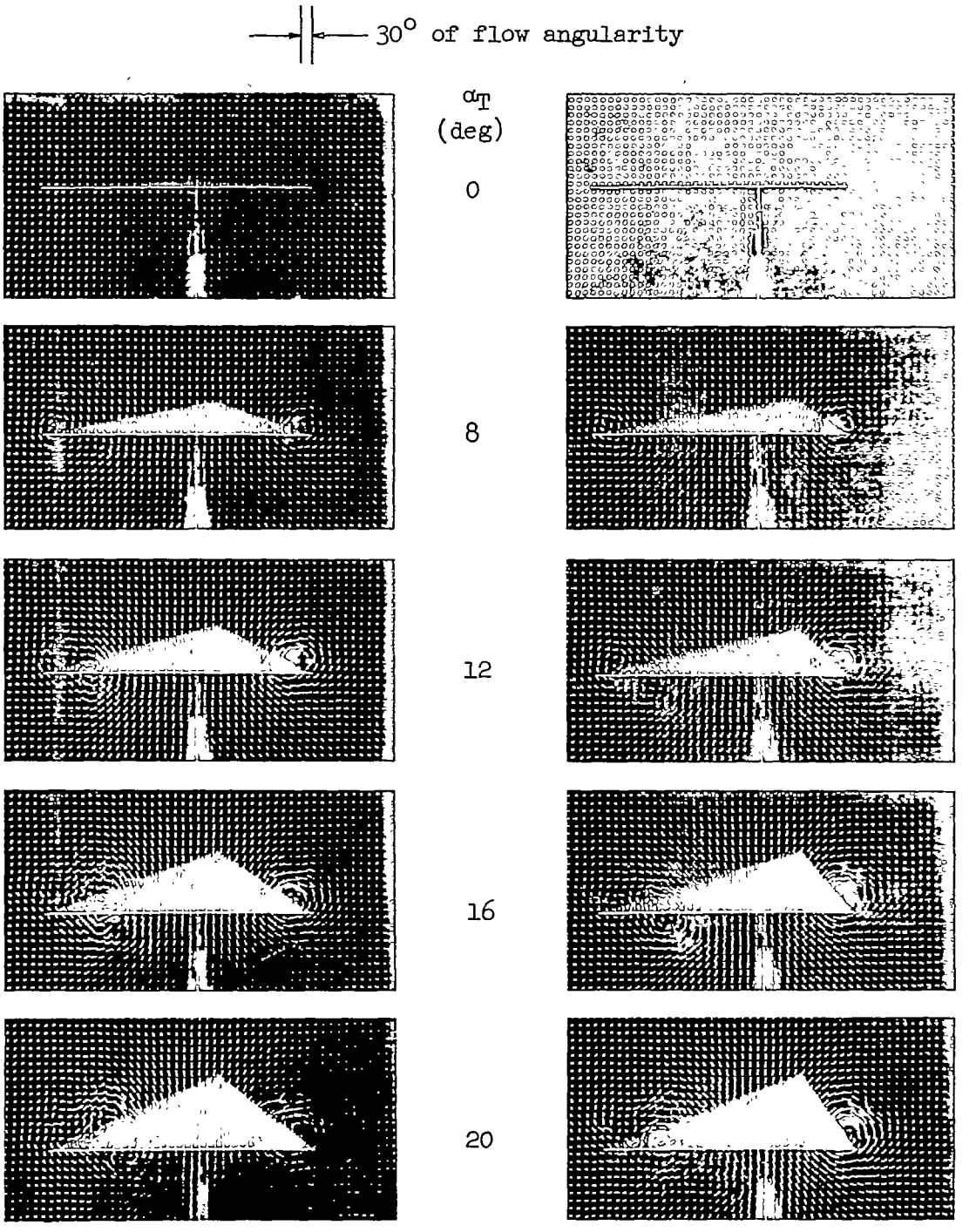


(c) $\beta = -10^{\circ}$.

(d) $\beta = -20^{\circ}$.

Figure 14.- Concluded.

NACA
L-72728

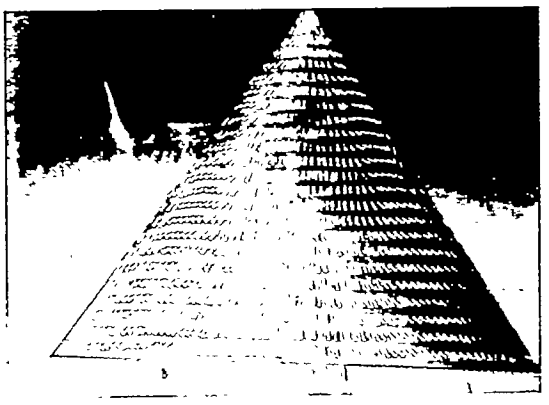

$\beta = 0^{\circ}$

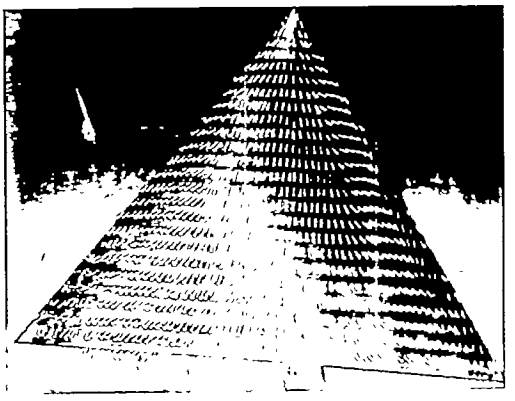

$\beta = -5^{\circ}$

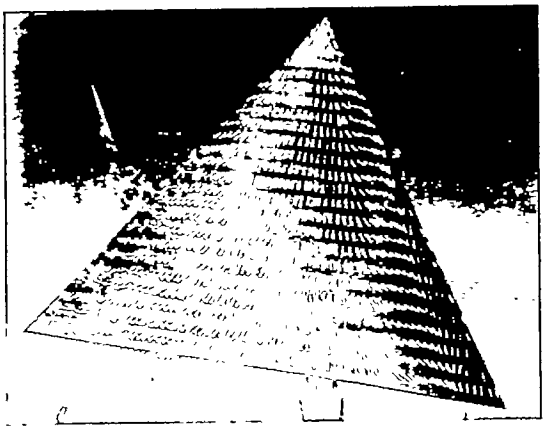

$\beta = -10^{\circ}$

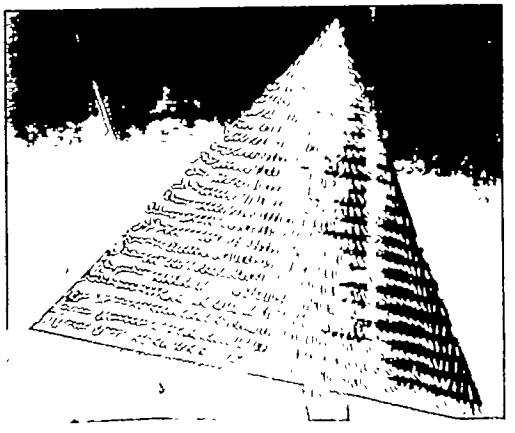

$\beta = -15^{\circ}$

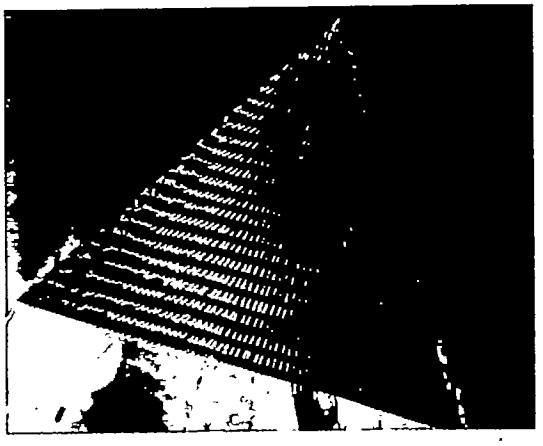

$\beta = -20^{\circ}$

L-72729

Figure 15.- Surface-tuft photographs for a $60^{\circ}$ triangular wing having an NACA $65_{(06)}$-006.5 airfoil section at $\alpha_T = 20^{\circ}$ for various angles of sideslip.

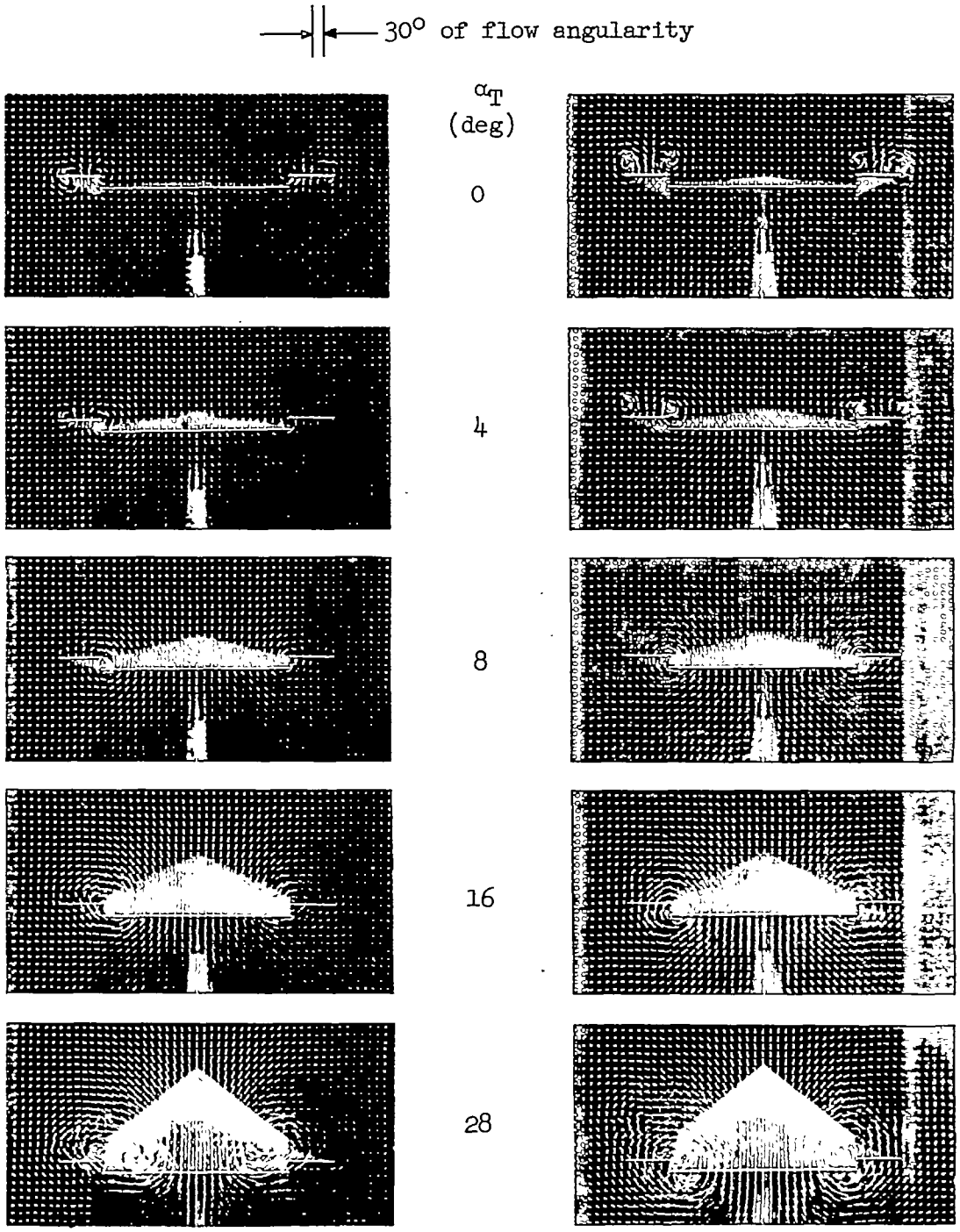


(a) Tuft grid 6 inches from trailing edge.

(b) Tuft grid 24 inches from trailing edge.

Figure 16.- Tuft-grid photographs for a 60° triangular wing having an NACA $65_{(06)}$-006.5 airfoil section and with 10-percent half-delta all-moving tip controls deflected -20° for two stations behind wing. $\beta = 0°$.

L-72730

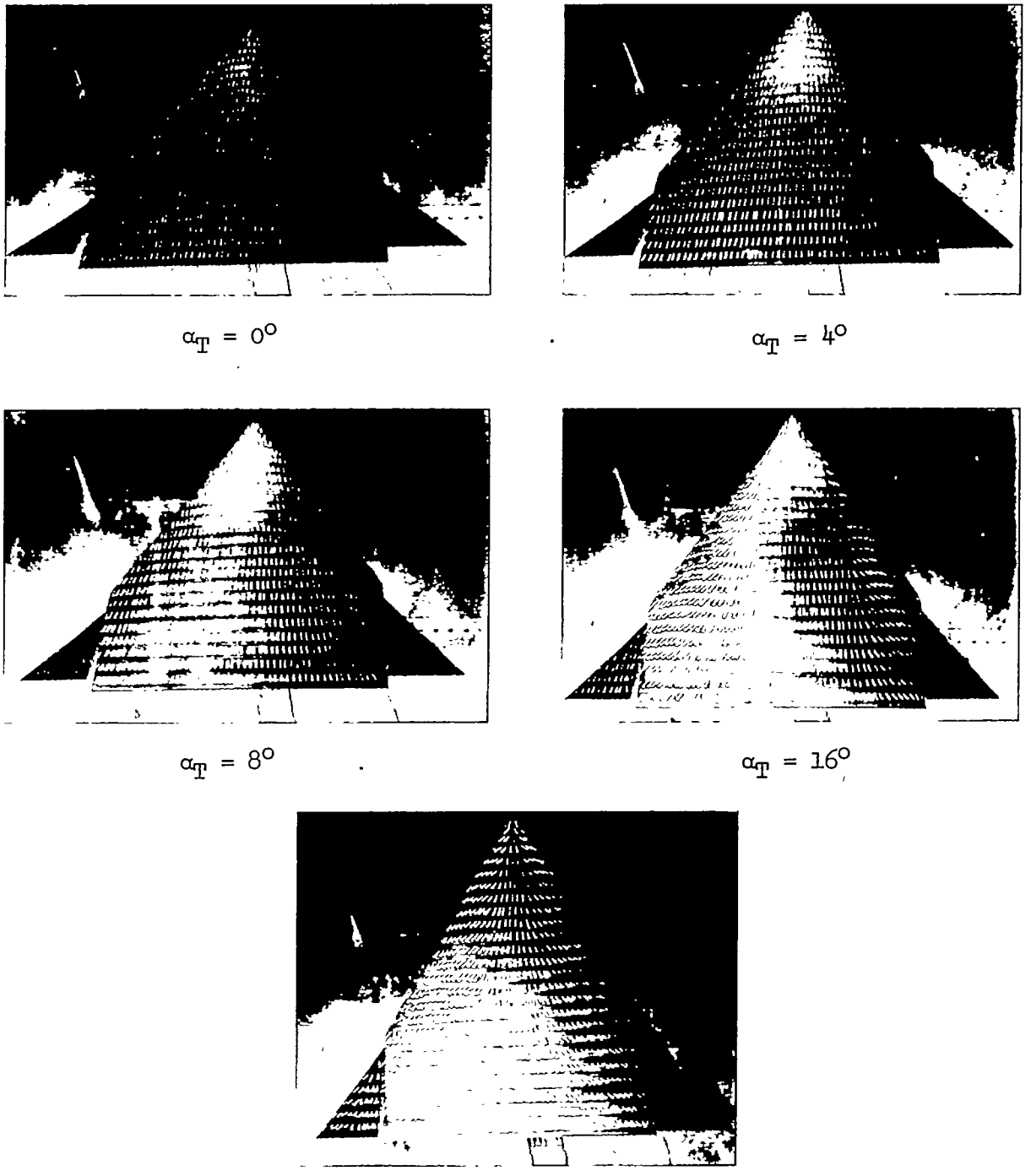


NACA
L-72731

Figure 17.- Surface-tuft photographs for a 60° triangular wing having an NACA $65_{(06)}$-006.5 airfoil section with 10-percent half-delta all-moving tip controls deflected -20°. $\beta = 0^\circ$.

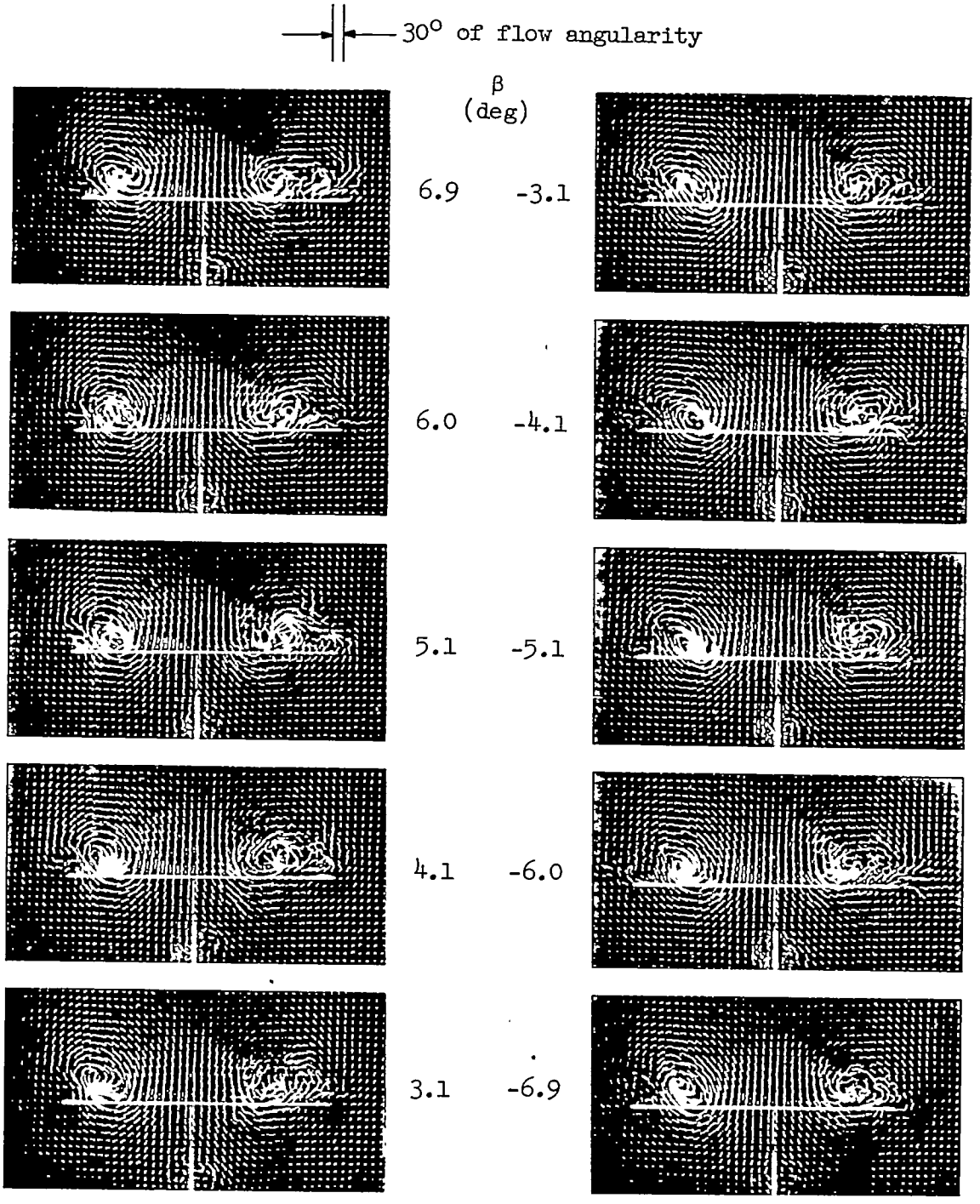


(a) Frames 1 to 5.

(b) Frames 11 to 15.

Figure 18.- Tuft-grid photographs for a 60° triangular wing having a flat-plate section at 21° angle of attack oscillating at 1 cycle per second through a sideslip range of ±12°. Tuft grid located 6 inches from trailing edge.

L-72732

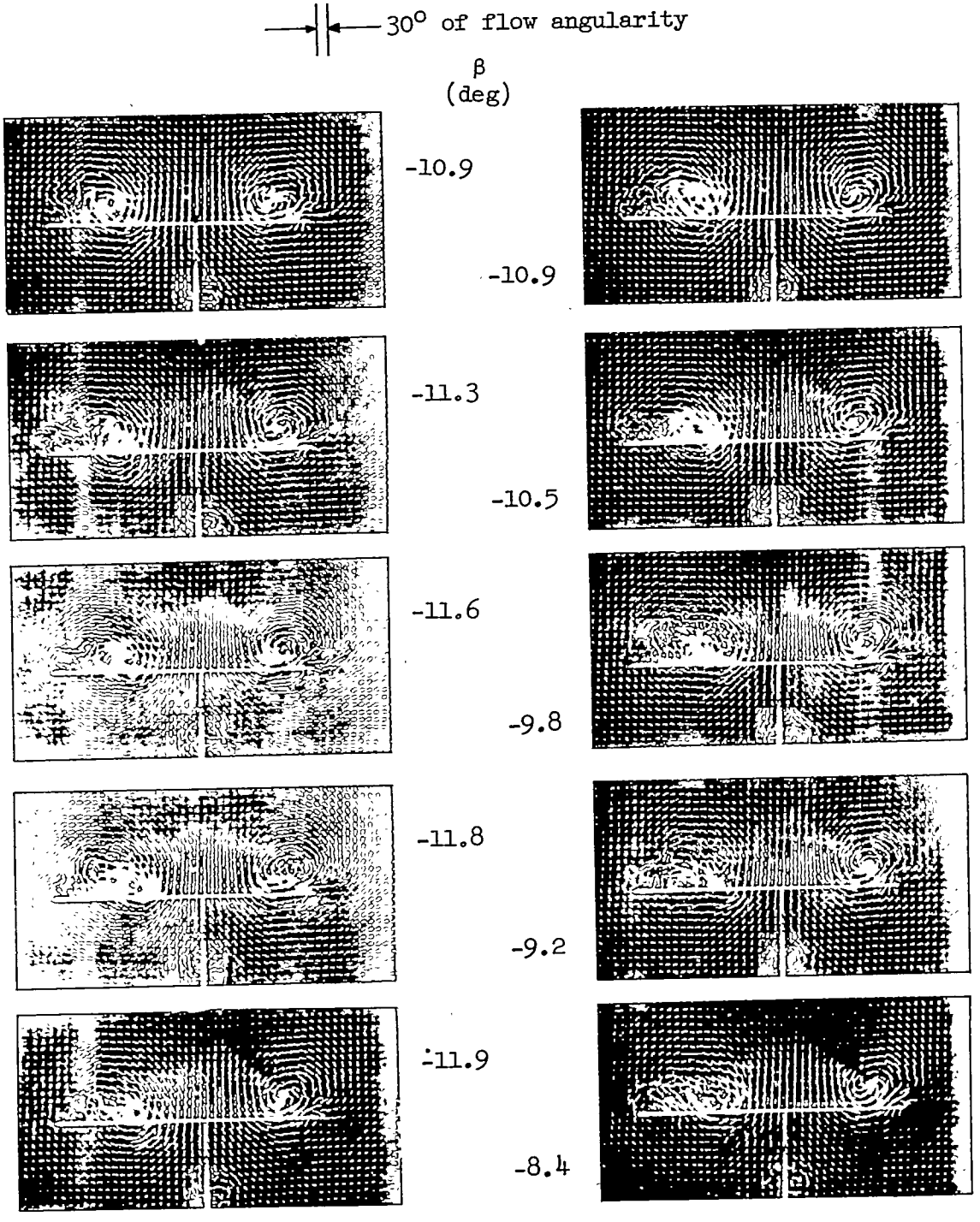


(c) Frames 21 to 25.

(d) Frames 31 to 35.

Figure 18.- Concluded.

L-72733